

Combined Effects of Hall Current and Heat Transfer on Peristaltic Transport of a Nanofluid in a Vertical Tapered Channel Through a Porous Medium

Ahmed I. Abdellateef and Syed Z. Ul Haque*

Department of Mathematics and Statistics, Caledonian College of Engineering, Sultanate of Oman, Muscat. University of Glasgow, Scotland, UK. *Email: hqzahoor@gmail.com.

ABSTRACT: The influences of Hall currents and heat transfer on peristaltic transport of a nanofluid in a vertical porous tapered channel through a porous medium are investigated theoretically and graphically under the assumptions of low Reynolds number and long wavelength and the flow investigated is in a wavy frame of reference. Analytical solutions are obtained for temperature, axial velocity, stream function and pressure gradient. Graphical results are sketched for various embedded parameters.

Keywords: Peristaltic flow; Heat transfer; Nanofluid; Tapered channel; Hall currents and Porous medium.

التأثير المشترك لكل من الانتقال الحراري وتيارات الهول على النقل التمعجي لمائع نيوتوني عبر قناة رأسية مستطيله في وسط مسامي

أحمد إبراهيم عبد اللطيف و سيد زهورالحق

مستخلص: تم دراسة التأثير المشترك لكل من الانتقال الحراري وتيارات الهول كرننت على النقل التمعجي لمائع نيوتوني عبر قناة رأسية مستطيله في وسط مسامي. تمت الدراسة نظريا واستنتجت الرسومات بناءً على فرضية صغرى عدد رينولد وكبير الطول الموجي. تمت دراسة السريان عبر اطار الاسناد الموجي. وتم حساب دالة التوزيع الحراري والسرعة المحورية ودالة السريان وكذلك تدرج الضغط خلال السريان. وتم مناقشة واطهار النتائج المستخلصة من خلال الرسومات المختلفة.

كلمات مفتاحية: نقل تمعجي ، انتقال حراري ، مائع نانوي ، قناة متباعدة ، تيارات هول و وسط مسامي.

1. Introduction

Mass transfer and heat transfer from different geometries embedded in a porous medium have many geophysical and engineering applications such as thermal insulations, drying of porous solids, cooling of nuclear reactors, underground energy transport, and crude oil extraction. The study of fluid flow through a porous medium and heat transfer constitute a fundamental study of nature and have great practical importance in several physical problems; these include porous heat exchangers, sewage of water in river beds, filtration and purification processes, for example. Their industrial importance has led to many experimental and analytical studies of flow and heat transfer in a porous medium in the presence of a magnetic field. McWhirter *et al.* [1], and Geindreau and Auriault [2] have discussed magnetohydrodynamic (MHD) flow through a porous medium in great details. The tapered channel is specially designed to assist in the management of subglottic, tracheal, and glottic stenosis. The superior end conforms to the contours of the glottis, while the larger inferior portion simultaneously acts as a stent for the trachea. The design of the tapered end is such that it projects up beyond the true vocal cords to the level of the laryngeal ventricle. Peristaltic flow is a phenomenon found in several industrial and physiological processes. Within the body peristaltic flows occur widely in fluid processes such as in urine transport from kidney to bladder through the ureter, transport of lymph in the lymphatic vessels, swallowed food through the esophagus, spermatozoa transport in the human reproductive tract, vaso motion of small blood vessels, etc. In addition to that, peristaltic pumping occurs in many practical applications involving biomechanical systems. The mechanism of peristaltic flow can be best explained by comparing the experimental clinical data and mathematical results. A perfect mathematical study can be served to many peristaltic flows occurring in the human body. Many research attempts had been made to understand peristaltic action in different situations. The first attempt was made by Latham [3] and some of the interesting investigations in the same direction are given in references [4–7]. Moreover, the flow through a porous medium has also attracted the attention of many

researchers in the past few decades because of its important practical applications, as it occurs in sandstone, limestone, filtration of fluids and seepage of water in river beds, wood, and in human lungs, the bile duct, the gall bladder with stones, and in small blood vessels etc. Shehawey *et al.* [8] formulated a mathematical model for the peristaltic transport of a viscous incompressible fluid through a porous medium bounded by two porous plates and El Shehawey *et al.* [9] studied the peristaltic transport in an asymmetric channel through a porous medium. Vajravelu *et al.* [10] examined peristaltic flow through vertical porous tube. Srinvas and Kothandapani [11] investigated the influence of heat and mass transfer on MHD peristaltic flow through a porous space with compliant walls. Srinvas and Gayathri [12] continued this work and discussed the peristaltic transport of Newtonian fluid in an asymmetric channel of a porous medium with heat transfer. The Hall effect is important when the Hall parameter which is the ratio between the electron-cyclotron frequency and the electron-atom-collision frequency is high. This can occur if the collision frequency is low or when the magnetic field is high. This is a current trend in MHD because of the important influence of the electromagnetic force. There has been considerable study of Hall effects and heat transfer effects on flow to determine the efficiency of certain devices such as heat exchangers and power generators. Attia [13] examined unsteady Hartmann flow with heat transfer of a viscoelastic fluid taking the Hall effect into consideration. Asghar *et al.* [14] studied the effects of Hall current and heat transfer on flow due to the pull of an eccentric rotating disk. Hayat *et al.* [15] studied the Hall effects on peristaltic flow of a Maxwell fluid in a porous medium. Abo-Eldahab *et al.* [16, 17] investigated the effects of Hall and ion-slip currents on MHD peristaltic transport and couple stress fluid. For further information the references [18–25] provide additional source.

The aim of this paper is to investigate the effects of Hall current and heat transfer on peristaltic transport of a Newtonian nanofluid in a tapered channel through a porous medium.

Nomenclature

a_1, b_1	Wave amplitudes	R_e	Reynolds number
d_1+d_2	Two-dimensional channel width	δ	Dimensionless wave number
λ	Wavelength of the peristaltic wave	m_1	Hall current parameter
c_1	Wave speed	M	Magnetic field parameter
ϕ	Phase difference	\hat{k}	Thermal conductivity
ρ_f	Density of the fluid	N_t	Thermophoresis parameter
ρ_p	Density of the particle	N_b	Brownian motion parameter
\vec{q}	Velocity vector	G_r	Thermal Grashof number
T_s	Fluid temperature in static condition	B_r	Local nanoparticle Grashof number
D/Dt	Material derivative	Δp	Pressure rise
\bar{p}	Pressure	F_λ	Friction force
\bar{C}	Nanoparticle volume fraction	K	Porosity parameter
D_B	Brownian diffusion coefficient	θ	Temperature distribution
D_T	Thermophoretic diffusion coefficient	σ	Dimensionless nanoparticle volume fraction
d	Amplitude ratio		

2. Formulation of the problem

Consider the peristaltic transport of a nanofluid in a two-dimensional channel of width $(d_1 + d_2)$. The flow is induced by propagating a sinusoidal wave with constant speed ‘ c ’ along the channel walls (as shown in Fig. 1). We denote the channel walls by H_1 and H_2 .

$$H_1(\bar{X}, \bar{t}) = d_1 + K_1 x + a_1 \cos\left[\frac{2\pi}{\lambda}(X - c_1 t)\right] \quad \text{Right wall} \quad (1)$$

$$H_2(\bar{X}, \bar{t}) = -d_2 - K_2 x - b_1 \cos\left[\frac{2\pi}{\lambda}(X - c_1 t) + \phi\right] \quad \text{Left wall} \quad (2)$$

where a_1 and a_2 are the wave’s amplitudes, λ is the wave length, c_1 is the wave speed, and ϕ ($0 \leq \phi \leq \pi$) is the phase difference. It should be noted that $\phi = 0$ corresponds to a symmetric channel with waves out of phase and that

COMBINED EFFECTS OF HALL CURRENT AND HEAT TRANSFER

for $\phi = \pi$ the waves are in phase. Further, d_1, d_2, a_1, b_1 and ϕ satisfy the following inequality $a_1^2 + b_1^2 + 2a_1b_1 \cos \phi \leq (d_1 + d_2)^2$. The walls $Y = H_1$ and $Y = H_2$, are maintained at temperatures T_1 and T_2 respectively.

The governing equations for the flow and heat transfer of an incompressible nanofluid in the absence of body force are:

$$\bar{\nabla} \cdot \bar{q} = 0, \quad (3)$$

$$\rho_f \frac{D\bar{q}}{Dt} = -\bar{\nabla} \bar{p} + \mu \bar{\nabla}^2 \bar{q} + \bar{f}, \quad (4)$$

$$(\rho c)_f \frac{D\bar{T}}{Dt} = k \bar{\nabla}^2 \bar{T} + (\rho c)_p [D_B (\bar{\nabla} C) \cdot (\bar{\nabla} \bar{T}) + \frac{D_T}{(T_0)} (\bar{\nabla} \bar{T}) \cdot (\bar{\nabla} \bar{T})], \quad (5)$$

$$\frac{D\bar{C}}{Dt} = D_B \bar{\nabla}^2 \bar{C} + \frac{D_T}{(T_0)} \bar{\nabla}^2 \bar{T}, \quad (6)$$

where ρ_f is the density of the fluid, ρ_p is the density of the particle, \bar{q} is the velocity vector, \bar{f} is the body force, T_s is the fluid temperature in static condition, $\frac{D}{Dt}$ represents the material derivative, \bar{p} is the pressure, \bar{C} is the nanoparticle volume fraction, D_B is the Brownian diffusion coefficient and D_T is the thermophoretic diffusion coefficient. We now introduce a wavy frame (x, y) moving with velocity c_1 away from the fixed frame (X, Y) by the transformation

$$x = X - c_1 t, y = Y, u = U - c_1, v = V, p(x) = P(X, t), \quad (7)$$

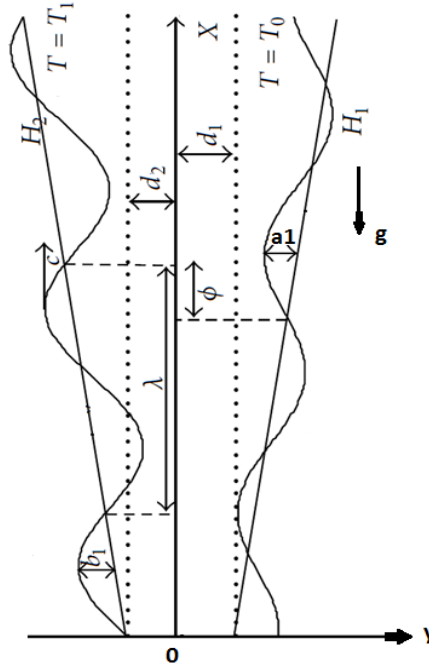


Figure 1. The simplified model geometry of the problem.

where (u, v) are the velocity components in the wavy frame (x, y) , p and P are pressures in wavy and fixed frame respectively. The pressure p remains constant across any axial station of the channel under the assumption that the wavelength is large and the curvature effects are negligible. After using these transformations, the governing equations in steady case become:

$$\frac{\partial \bar{u}}{\partial x} + \frac{\partial \bar{v}}{\partial y} = 0, \quad (8)$$

$$\rho[\bar{u} \frac{\partial \bar{v}}{\partial \bar{x}} + \bar{v} \frac{\partial \bar{v}}{\partial \bar{y}}] = -\frac{\partial \bar{p}}{\partial \bar{y}} + \mu \left(\frac{\partial^2 \bar{v}}{\partial \bar{x}^2} + \frac{\partial^2 \bar{v}}{\partial \bar{y}^2} \right) - \frac{\mu^-}{k_1} \bar{v} - \frac{\sigma B_o^2}{(1+m_1^2)} (m_1 \bar{u} + \bar{v}) \quad (9)$$

$$\begin{aligned} \rho[\bar{u} \frac{\partial \bar{u}}{\partial \bar{x}} + \bar{v} \frac{\partial \bar{u}}{\partial \bar{y}}] = & -\frac{\partial \bar{p}}{\partial \bar{x}} + \mu \left(\frac{\partial^2 \bar{u}}{\partial \bar{x}^2} + \frac{\partial^2 \bar{u}}{\partial \bar{y}^2} \right) \\ & + \rho g \beta (T - T_0) + \rho g \beta^* (C - C_0) - \frac{\mu^-}{k_1} \bar{u} + \frac{\sigma B_o^2}{(1+m_1^2)} (m_1 \bar{v} - \bar{u}) \end{aligned} \quad (10)$$

$$\begin{aligned} [\bar{u} \frac{\partial \bar{T}}{\partial \bar{x}} + \bar{v} \frac{\partial \bar{T}}{\partial \bar{y}}] = & \alpha \left(\frac{\partial^2 \bar{T}}{\partial \bar{x}^2} + \frac{\partial^2 \bar{T}}{\partial \bar{y}^2} \right) + \tau_r [D_B \{ (\frac{\partial \bar{C}}{\partial \bar{y}} \frac{\partial \bar{T}}{\partial \bar{y}}) + (\frac{\partial \bar{C}}{\partial \bar{x}} \frac{\partial \bar{T}}{\partial \bar{x}}) \} + \\ & \frac{D_T}{(T_0)} \{ (\frac{\partial \bar{T}}{\partial \bar{y}})^2 + (\frac{\partial \bar{T}}{\partial \bar{x}})^2 \}] \end{aligned} \quad (11)$$

$$[\bar{u} \frac{\partial \bar{C}}{\partial \bar{x}} + \bar{v} \frac{\partial \bar{C}}{\partial \bar{y}}] = D_B \left(\frac{\partial^2 \bar{C}}{\partial \bar{x}^2} + \frac{\partial^2 \bar{C}}{\partial \bar{y}^2} \right) + \frac{D_T}{(T_0)} \left(\frac{\partial^2 \bar{T}}{\partial \bar{x}^2} + \frac{\partial^2 \bar{T}}{\partial \bar{y}^2} \right) \quad (12)$$

where $\tau_r = \frac{(\rho c)_p}{(\rho c)_f}$ is the ratio between the effective heat capacity of the nanoparticle material and heat capacity of the fluid.

The corresponding no-slip boundary conditions are:

$$\begin{aligned} \bar{u} = -c_1, \bar{C} = C_1, \bar{T} = T_1 \text{ at } \bar{y} = \bar{H}_1, \\ \bar{u} = -c_1, \bar{C} = C_2, \bar{T} = T_2 \text{ at } \bar{y} = \bar{H}_2. \end{aligned} \quad (13)$$

Consider the following non-dimensional variables and parameters:

$$\begin{aligned} u = \frac{\bar{u}}{c_1}, v = \frac{\bar{v}}{\delta c_1}, x = \frac{\bar{x}}{\lambda}, y = \frac{\bar{y}}{d_1}, \delta = \frac{d_1}{\lambda}, p = \frac{d_1^2 \bar{p}}{\mu \lambda c_1}, t = \frac{c \bar{t}}{\lambda}, h_1 = \frac{\bar{H}_1}{d_1}, h_2 = \frac{\bar{H}_2}{d_1}, \\ d = \frac{d_2}{d_1}, b = \frac{a_2}{d_1}, a = \frac{a_1}{d_1}, P_r = \frac{\nu}{\alpha}, R_e = \frac{c_1 d_1}{\nu}, \theta = \frac{T - T_s}{T_1 - T_s}, N_t = \frac{(\rho c)_p D_T (T_1 - T_s)}{(\rho c)_f \alpha}, \\ \sigma = \frac{(\bar{C} - \bar{C}_0)}{\bar{C}_0}, N_b = \frac{(\rho c)_p D_B \bar{C}_0}{(\rho c)_f \alpha}, \alpha = \frac{\hat{k}}{(\rho c)_f}, G_r = \frac{g \beta d_1^2 (T_1 - T_s)}{\nu c}, \\ B_r = \frac{g \beta^* d_1^2 \bar{C}_0}{\nu c}, k = \frac{\bar{k}_1}{a^2}, M = \frac{\sigma B_o^2 d_1^2}{\mu}, k_1 = \frac{K_1}{d_1}, k_2 = \frac{K_2}{d_1} \end{aligned} \quad (14)$$

where T_s - the fluid temperature in static condition, d - the amplitude ratio, R_e - the Reynolds number, δ - the dimensionless wave number, m_1 - the Hall current parameter, M - the magnetic field parameter, \hat{k} - the thermal conductivity, and N_b , N_t , B_r and G_r are the Brownian motion parameter, thermophoresis parameter, local nanoparticle Grashof number, and local thermal Grashof number respectively.

With the help of Eq. (2.14) in Eqs.(2.8)–(2.13) under the assumptions of long wavelength and low Reynold number approximation takes the form

$$\frac{\partial u}{\partial x} + \frac{\partial v}{\partial y} = 0, \quad (15)$$

$$\frac{\partial p}{\partial y} = 0 \quad (16)$$

$$\frac{\partial p}{\partial x} = \frac{\partial^2 u}{\partial y^2} + G_r \theta + B_r \sigma - \left(\frac{1}{k_1} + \frac{M}{(1+m_1^2)} \right) u \quad (17)$$

$$0 = \frac{\partial^2 \theta}{\partial y^2} + N_b \left(\frac{\partial \sigma}{\partial y} \frac{\partial \theta}{\partial y} \right) + N_t \left(\frac{\partial \theta}{\partial y} \right)^2 \quad (18)$$

$$0 = \frac{\partial^2 \sigma}{\partial y^2} + \frac{N_t}{N_b} \frac{\partial^2 \theta}{\partial y^2} \quad (19)$$

The corresponding boundary conditions become:

$$\begin{aligned} u &= -1, & \theta &= 1, & \sigma &= 0, & y &= h_1, \\ u &= -1, & \theta &= m_0, & \sigma &= 0, & y &= h_2, \end{aligned} \quad (20)$$

where $m_0 = (T_2 - T_s)/(T_1 - T_s)$, the wall temperature ratio.

The solution of Eqs. (2.18,2.19), valid in $h_2 \leq y \leq h_1$ satisfying the corresponding boundary conditions (20) is given by

$$\theta = 1 + A_1 \left(e^{-s_1 N_b y} - e^{-s_1 h_1 N_b} \right) \quad (21)$$

$$\sigma = \frac{N_t}{N_b} (1 - \theta) + s_1 (y - h_1) \quad (22)$$

By substituting Eqs. (2.21)-(2.22) in Eq. (2.17) and solving it analytically as a second order ordinary differential equation, we get a solution in the form,

$$u(x) = c_2 + c_3 y + c_4 e^{-\sqrt{A_2} y} + c_5 e^{\sqrt{A_2} y} + c_6 e^{-s_1 N_b y} \quad (23)$$

3. Rate of volume flow

The instantaneous volume flow rate in the fixed frame is given by

$$Q = \int_{\bar{H}_2}^{\bar{H}_1} \bar{U}(\bar{X}, \bar{Y}, \bar{t}) d\bar{Y}, \quad (3.1)$$

where \bar{H}_1 and \bar{H}_2 are functions of X, t .

The rate of volume flow in the wave frame is given by

$$q = \int_{\bar{H}_2}^{\bar{H}_1} \bar{u}(\bar{x}, \bar{y}) d\bar{y}, \quad (3.2)$$

where h_1 and h_2 are the functions of x alone. If we substitute equation (1.7) into (2.1) and make use of (2.2), it is found that the related rates of volume flow is:

$$Q = q + c_1 \bar{H}_1 - c_1 \bar{H}_2. \quad (3.3)$$

The time-mean flow over a period T at a fixed position X is defined as:

$$Q^* = \frac{1}{T} \int_0^T Q dt, \quad (3.4)$$

Substituting (2.3) into (2.4), and integrating, we get:

$$Q^* = q + c_1 d_1 + c_1 d_2. \quad (3.5)$$

On defining the dimensionless time-mean flows \bar{Q} and \bar{q} in the fixed and wavy frame respectively as:

$$\bar{Q} = \frac{Q^*}{c_1 d_1} \quad \text{and} \quad \bar{q} = \frac{q}{c_1 d_1}, \quad (3.6)$$

One finds that (2.5) may be written as:

$$\bar{Q} = \bar{q} + 1 + d. \quad (3.7)$$

From Eq. (2.23), with the help of Eqs. (3.1)-(3.7), we get the pressure gradient. The pressure rise Δp and the friction force F_λ (at the walls) for a channel of length L , in their non-dimensional forms, are given by

$$\Delta p = \int_0^1 \frac{\partial p}{\partial x} dx, \quad (3.8)$$

$$F_\lambda^{h_1} = \int_0^1 (-h_1^2 \frac{\partial p}{\partial x}) dx. \quad (3.9)$$

$$F_\lambda^{h_2} = \int_0^1 (-h_2^2 \frac{\partial p}{\partial x}) dx. \quad (3.10)$$

The integrals in equations (3.9)-(3.10) are not integrable in closed form, they are evaluated numerically using a ready package of Nintegrate Library from Mathematica 7.

Nintegrate uses an algorithm called ‘integration strategies’ that attempts to compute an integral which satisfy user specified precision or accuracy goals.

The corresponding stream functions ($u = \frac{\partial \psi}{\partial y}$, $v = -\frac{\partial \psi}{\partial x}$) are evaluated with boundary condition $\psi = 0$ at

$$z = \frac{1}{2}(h_1 + h_2).$$

4. Graphical results and discussion

Here we discuss the quantitative effects of sundry parameters used in analysis with the help of graphs and results. First, let us discuss the variations observed for the pressure rise distributions versus the time average flux (\bar{Q}), for different values of the local nanoparticle Grashof number (B_r), local thermal Grashof number (G_r), porosity parameter (K), thermophoresis parameter (N_t), non-uniform parameters (k_1) and (k_2), Hall parameter (M). It is noticed in Figure 2(a) that with an increase in the local nanoparticle Grashof Number (B_r), pressure rise reduces but Figure 2(b) shows the opposite behavior and pressure rise increases with the increase in the thermal Grashof number (G_r). At the same time Figure 2(c) shows the pressure rise plunges with the increase in porosity parameter (K), showing anticlockwise rotation in the graph. Figure 2(d) shows that with an increase in the thermophoresis number (N_t) pressure rise reduces. Figures 2(e) and 2(f) give the effect of the non-uniform parameters (k_1) and (k_2) on the pressure rise in the flow, and show that it plunges with the increase of the non-uniform parameters (k_1) and (k_2) showing anticlockwise rotation in the graph. In the retrograde pumping region the pressure rise decreases with an increase in non-uniform parameters (k_1) and (k_2). Finally, in Figure 2(g) the Hall parameter (M) gives the opposite effect to the porosity parameter (K), where the pressure rise increases in the retrograde quadrant with an increase in Hall parameter (M) and goes in clockwise rotation.

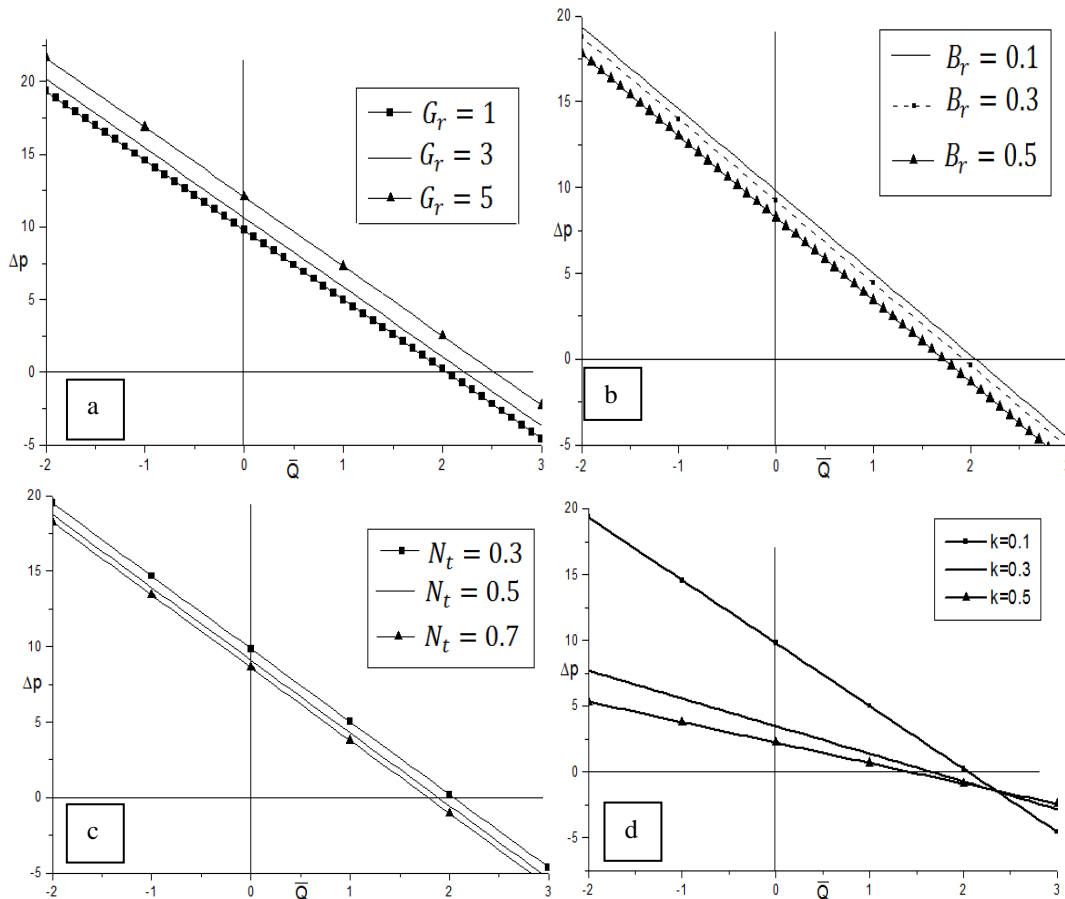


Figure 2. Variation of pressure rise over the length versus \bar{Q} .

COMBINED EFFECTS OF HALL CURRENT AND HEAT TRANSFER

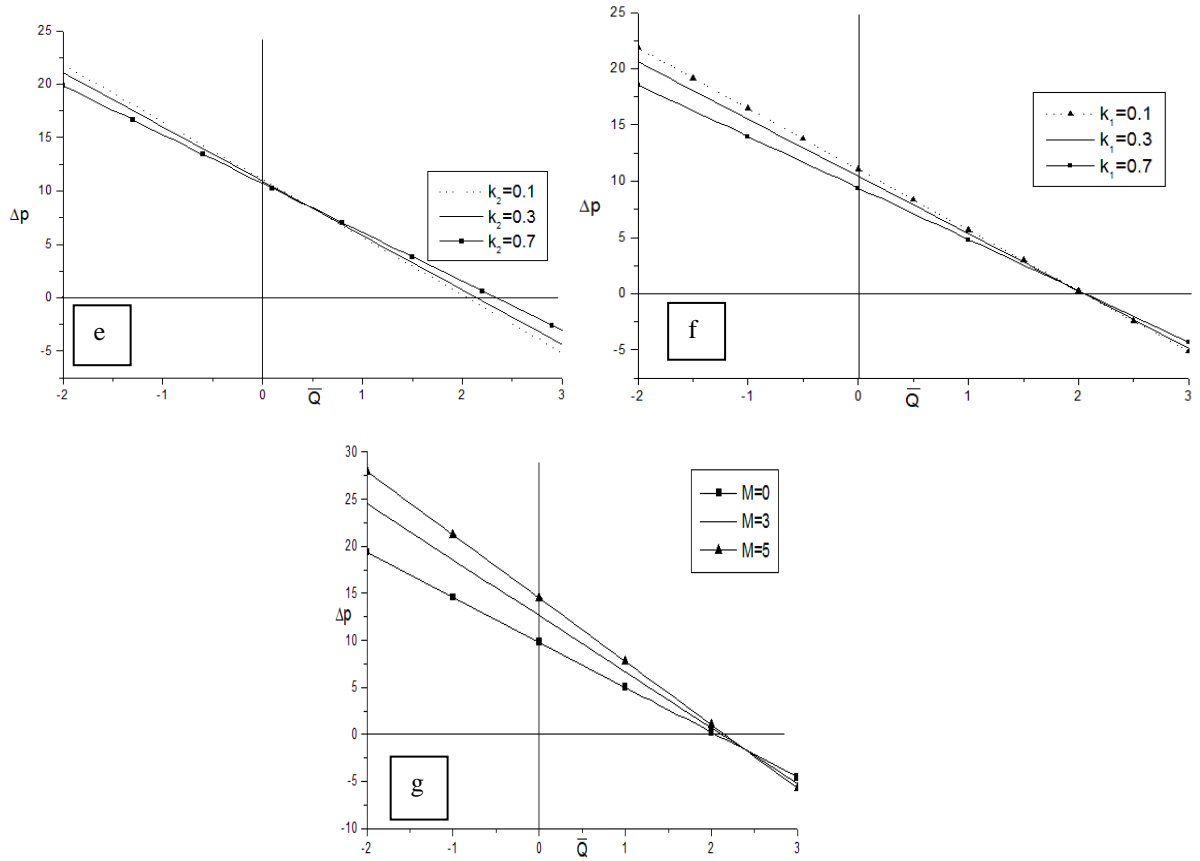


Figure 2. Contd.

A fluid particle that moves with a velocity that is different from its neighbours will be subjected to a frictional force, such forces also exist between a particle and a rigid boundary. The friction forces F_{λ}^1 and F_{λ}^2 on the right and left walls respectively can be obtained by integral evaluations of the analytic results gained for the pressure gradient $\frac{dp}{dx}$. The average of the right friction force (on the right flexible wall) as well as the average of the left friction force (on the left flexible wall) are plotted in Figure 3.

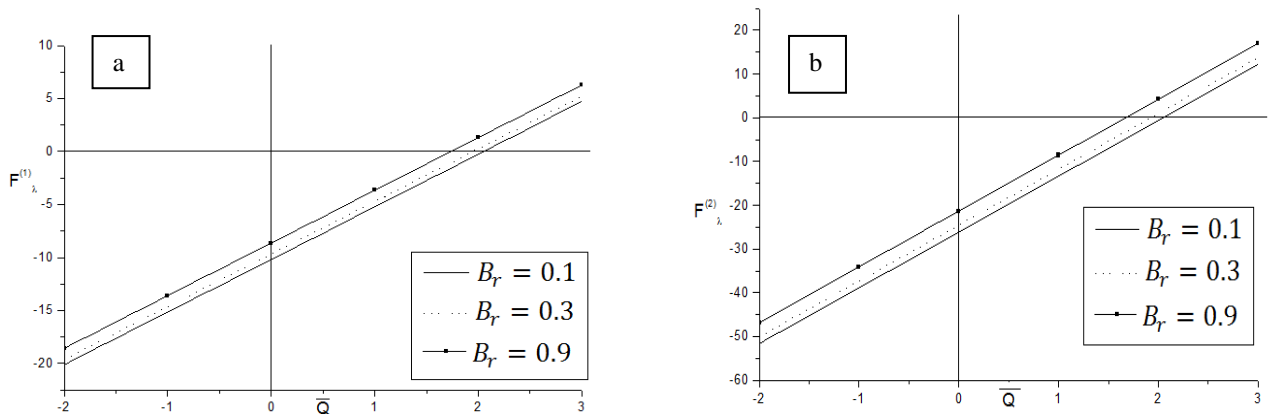


Figure 3. Variation of frictional forces.

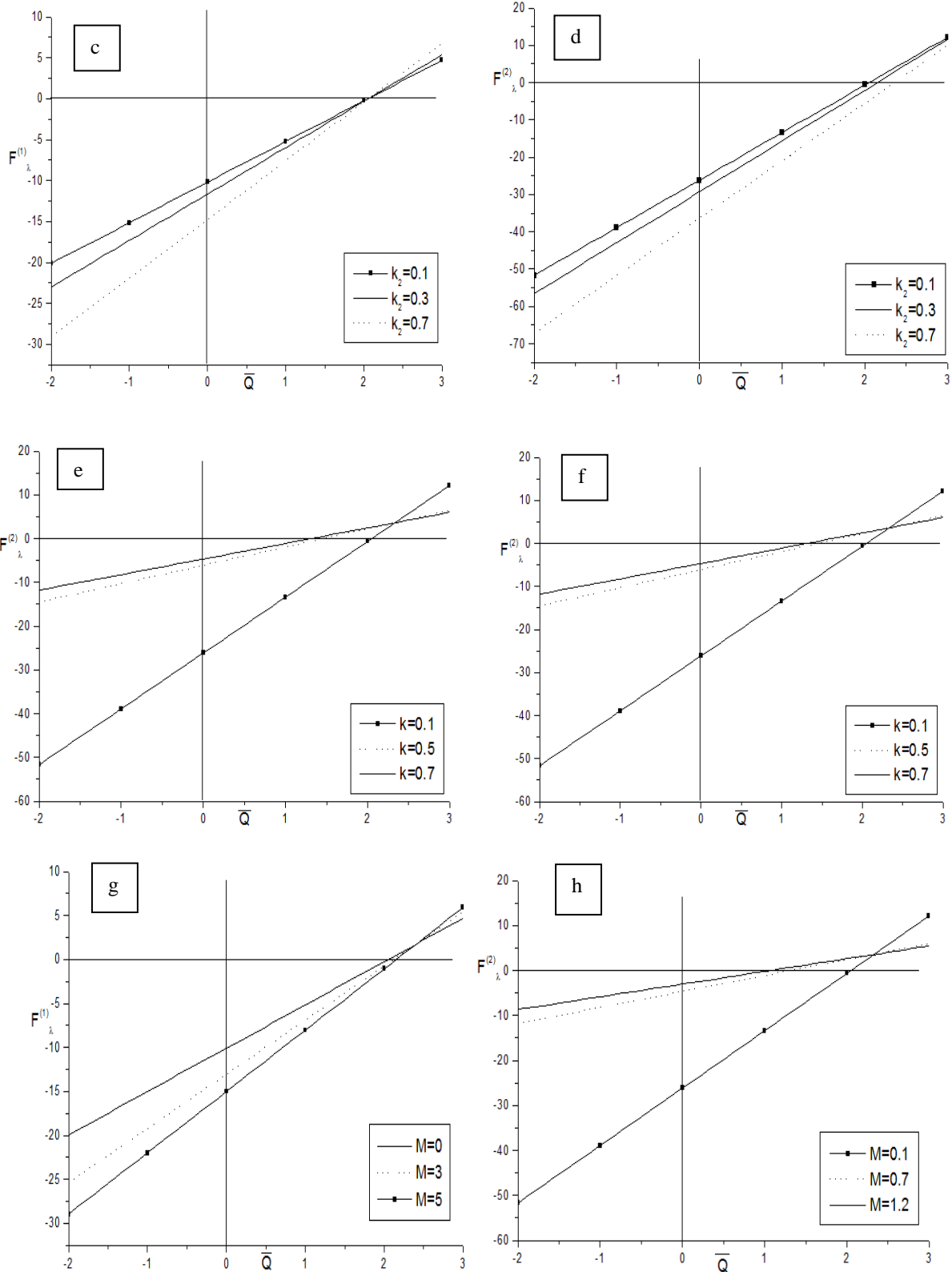


Figure 3. Contd.

We notice from these figures that the right and left wall friction forces have the opposite behavior as compared to the pressure rise. The right friction force behaves similarly to the left friction force for the same values of the parameters; however, the absolute value of the right friction force is greater than that of the left friction force at the same values of the parameters.

Trapping is the development and transport of an internally circulating bolus of fluid. In this bolus a fluid travels along the wave as it propagates. The effect of the Hall parameter (M) on the trapping can be observed through Figure 4 where the size of the bolus reduces with an increase in Hall parameter (M). The influences of phase

COMBINED EFFECTS OF HALL CURRENT AND HEAT TRANSFER

difference (ϕ), porosity parameter (K), wall temperature ratio m_0 , non-uniform parameters (k_1) and (k_2), Hall parameter (M) and thermophoresis parameter (N_t) are analyzed through Figures (4) and (5). We notice that the size of the trapped bolus increases with an increase in porosity parameter (K) and wall temperature ratio m_0 but it reduces with an increase in thermophoresis parameter (N_t) and the Hall parameter (M). We can also observe that streamlines get shifted due to the change in the values of phase difference (ϕ) and wall temperature ratio m_0 , and non-uniform parameter (k_1) and (k_2).

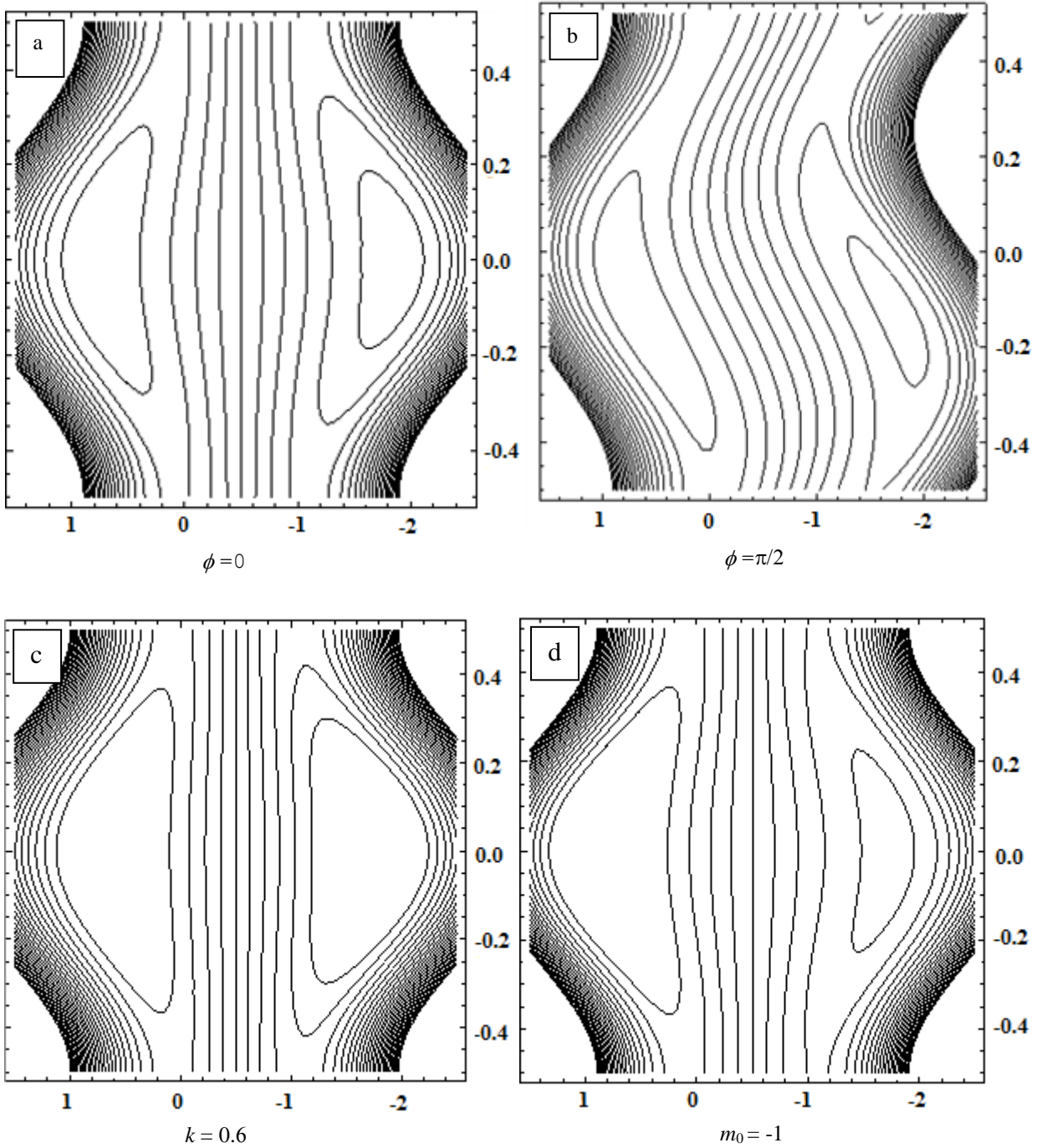


Figure 4. Streamlines for different values of ϕ , k , m_0 when $N_t = 0.2$, $N_b = 0.4$, $Q = 0.4$, $B_r = 0.4$, $G_r = 0.6$, $m = 0$, $k_1 = 0$, $k_2 = 0$.

Figure 6 depicts the variations of temperature profile (θ) and nanoparticle volume fraction (σ) for different values of the thermophoresis parameter (N_t), wall temperature ratio m_0 and non-uniform parameters (k_1) and (k_2). It is seen in Figures 6(c), 6(e) and 6(g) that the heat distribution (θ) increases with an increase in non-uniform parameter (k_2), thermophoresis parameter (N_t) and temperature ratio m_0 . On the other hand, Figures 6(b), 6(d), 6(f), and 6(h) show two different behaviour of the nanoparticles volume fraction (σ) profiles. It decreases with the increase of the thermophoresis parameter when $N_t < 0$, wall temperature ratio m_0 and non-uniform parameters (k_1) and (k_2). An opposite trend is observed when $N_t > 0$.

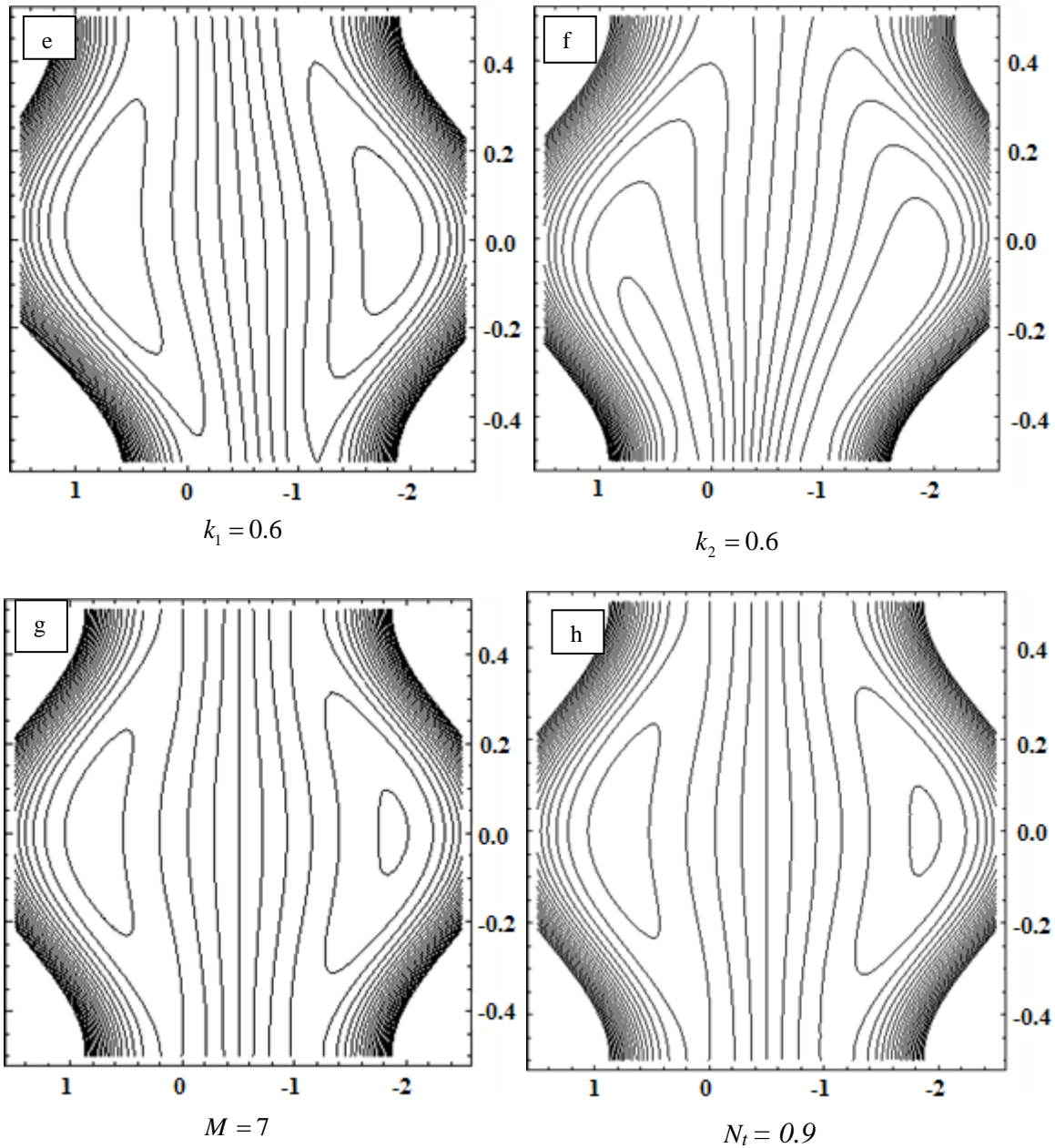


Figure 5. Streamlines for the different values of k_1, k_2, M, N_t when $N_b = 0.4, Q = 0.4, B_r = 0.4, G_r = 0.6, k = 0.2, m_0 = 2$.

COMBINED EFFECTS OF HALL CURRENT AND HEAT TRANSFER

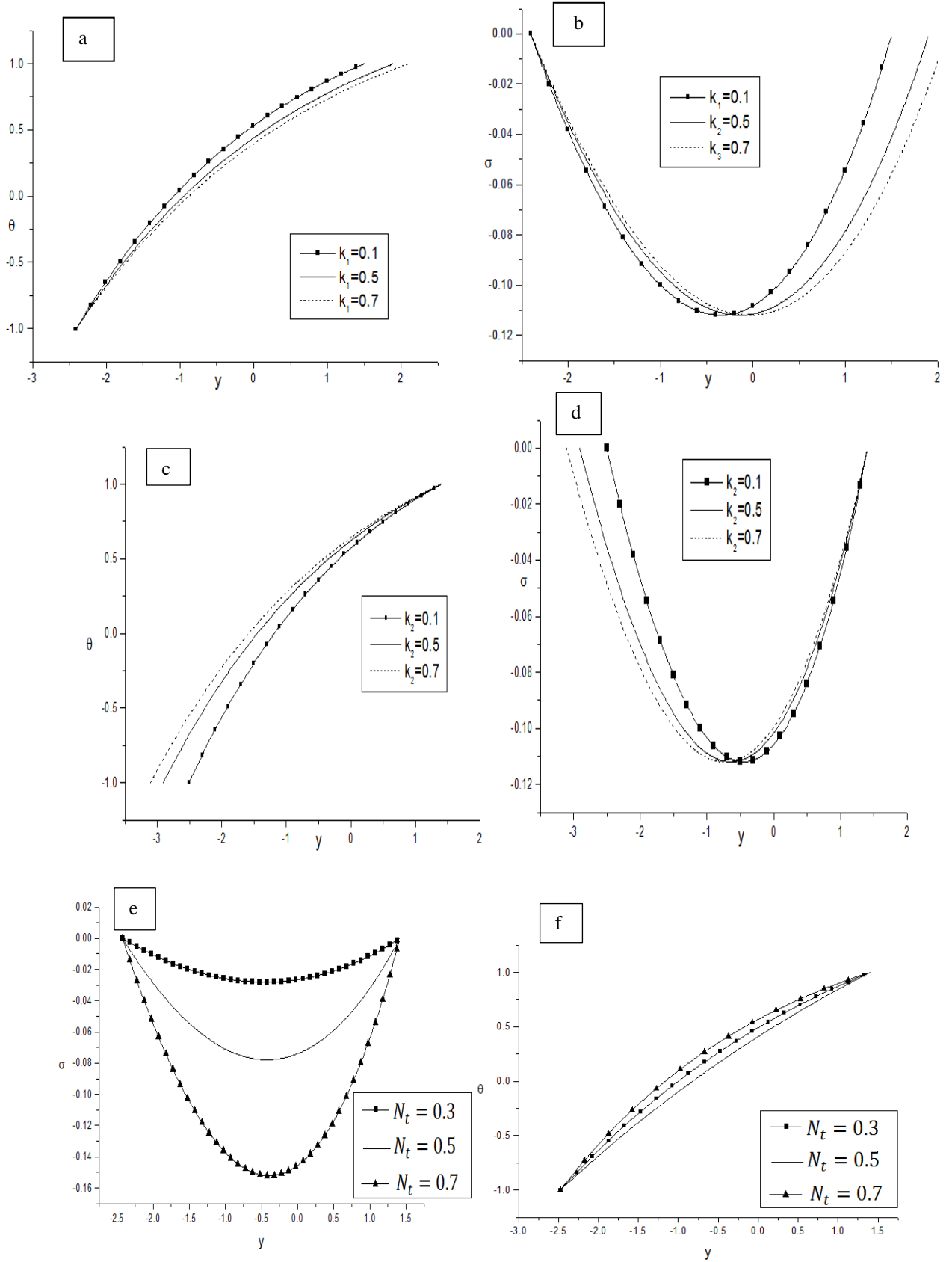


Figure 6. Concentration profile σ and heat distribution θ .

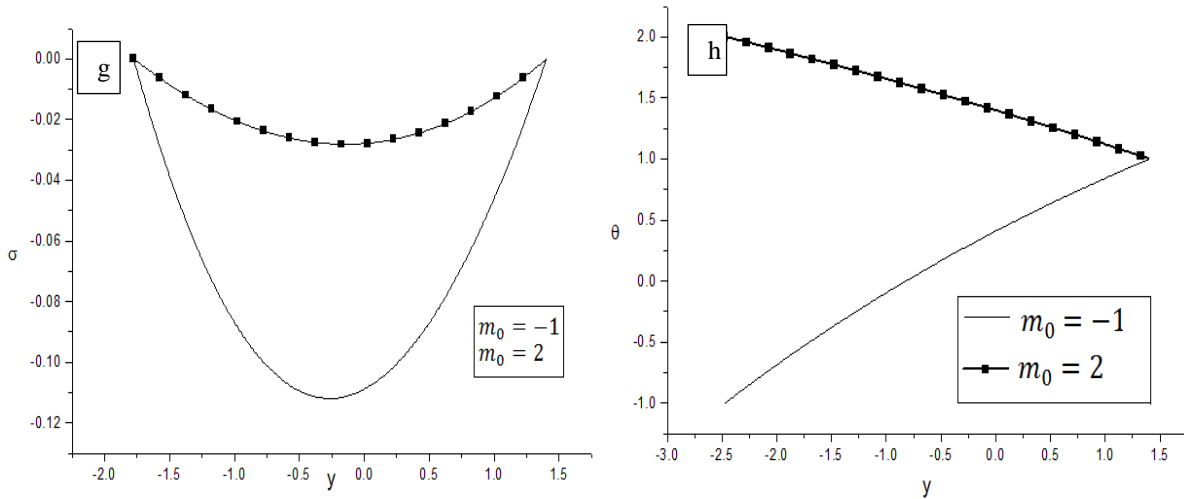


Figure 6. Contd.

6. Conclusion

The pressure rise reduces with an increase in the Hartmann number (M) and Thermophoresis parameter (N_t). It increases with the increase of the local nanoparticle Grashof number (B_r), local temperature Grashof number (G_r) and N_b . All these behaviors are in agreement with those reported by Kothandapani and Prakash [25]. The temperature distribution profile θ increases whereas nanoparticle concentration decreases with the increase of N_t and N_b .

References

1. Mc Whirter, J.D., Crawford, M.E. and Klein, D.E. Magnetohydrodynamic flows in porous media II: experimental results. *Fusion Technol.*, 1998, **34**, 187-197.
2. Geindreau, C. and Auriault, J.L. Magnetohydrodynamic flows in porous media. *J. Fluid Mech.*, 2002, **466**, 343-363.
3. Latham, T.W. Motion in a Peristaltic Pump, M.S. Thesis, MIT-Press, Cambridge, Mass, USA, 1966.
4. Fung, Y.C. and Yih, C.S. Peristaltic transport. *J. App. Mech.*, 1968, **35**, 669-675.
5. Shapiro, H., Jaffrin, M.Y. and Weinberg, S.L. Peristaltic pumping with long wavelengths at low Reynolds number. *J. Fluid Mech.*, 1969, **37**, 799-825.
6. Jaffrin, M.Y. and Shapiro, A.H. Peristaltic pumping. *Annual Rev. Fluid Mech.*, 1971, **3**, 13-36.
7. Srivastava, L.M. and Srivastava, V.P. Peristaltic transport of blood: Casson model II. *J. Biomech.*, 1984, **17**, 821-829.
8. El Shehawy, E.F., Eldabe, N.T., Elghazy, E.M. and Ebaid, A. Peristaltic transport in an asymmetric channel through a porous medium. *App. Math. Comp.* 2006, **182**, 140-150.
9. Vajravelu, K., Radhakrishnamacharya, G. and Radhakrishnamurthy, V. Peristaltic flow and heat transfer in a vertical porous annulus, with long wave approximation. *Int. J. Non-Linear Mech.*, 2007, **42**, 754-759.
10. Srinivas, S. and Kothandapani, M. The influence of heat and mass transfer on MHD peristaltic flow through a porous space with compliant walls. *App. Math. Comp.*, 2009, **213**, 197-208.
11. Srinivas, S. and Gayathri, R. Peristaltic transport of a Newtonian fluid in a vertical asymmetric channel with heat transfer and porous medium. *App. Math. Comp.*, 2009, **215**, 85-196.
12. Attia, H.A. Unsteady hartmann flow with heat transfer of a viscoelastic fluid considering the hall effect. *Canadian J. Phys.*, 2004, **82**, 127-139.
13. Asghar, S., Mohyuddin, M.R. and Hayat, T. Effects of Hall current and heat transfer on flow due to a pull of eccentric rotating disks. *Int. J. Heat Mass Trans.*, 2005, **48**, 599-607.
14. Hayat, T., Ali, N. and Asghar, S. Hall effects on peristaltic flow of a Maxwell fluid in a porous medium. *Phys. Lett. A.*, 2007, **363**, 397-403.
15. Abo-Eldahab, E.M., Barakat, E.I. and Nowar, K.I. Hall currents and ion-slip effects on the MHD peristaltic transport. *Int. J. App. Math. Phys.*, 2010, **2**, 113-123.
16. Abo-Eldahab, E.M., Barakat, E.I. and Nowar, K.I. Effects of Hall and ion-slip currents on peristaltic transport of a couple stress fluid. *Int. J. App. Math. Phys.*, 2010, **2**, 145-157.
17. Akbar, N.S. and Nadeem, S. Influence of heat transfer on peristaltic transport of a Johnson-Segalman fluid in an inclined asymmetric channel. *Commun. Nonlin. Sci. Numer. Simulat.*, 2010, **15**, 2860-2877.

18. Ali, N., Sajid, M., Javed, T. and Abbas, Z. Heat transfer analysis of peristaltic flow in a curved channel. *Int. J. Heat Mass Trans.*, 2010, **53**, 3319–3325.
19. Mekheimer, K.S., Saleem, N., Hayat, T. and Hendi, A.A. Simultaneous effects of induced magnetic field and heat and mass transfer on the peristaltic motion of second-order fluid in a channel. *Int. J. Numer. Meth. Fluid Flow.*, 2012, **70**, 342–358.
20. Mekheimer, K.S. and Abdel-Wahab, A.N. Net annulus flow of a compressible viscous liquid with peristalsis. *J. Aerospace Eng.*, 2012, **25**, 660–669.
21. Abd El-Maboud, Y. and Mekheimer, K.S. Non-linear peristaltic transport of a second-order fluid through a porous medium. *App. Math. Model.*, 2010, **35**, 2695–2710.
22. Mekheimer, K.S., Husseny, S.A. and Abd El-Maboud, Y. Effects of heat transfer and space porosity on peristaltic flow in a vertical asymmetric channel. *Numer. Meth. Partial Diff. Equa. Journal*, 2010, **26**, 747–770.
23. Gharsseidien, Z.M., Mekheimer, K.S. and Awad, A.S. The influence of slippage on trapping and reflux limits with peristalsis through an asymmetric channel. *App. Bionics Biomec.*, 2010, **7**, 95–108.
24. Srinivas, S. and Muthuraj, R. Effects of chemical reaction and space porosity on MHD mixed convective flow in a vertical asymmetric channel with peristalsis. *Math. Comp. Model.*, 2011, **54**, 1213–1227.
25. Kothandapani, M. and Prakash, J. Effect of radiation and magnetic field on peristaltic transport of nanofluid through a porous space in a tapered asymmetric channel. *J. Magnet. Mater.* 2015, **378**, 152–163.

Appendix

$$A_1 = \frac{1-m_0}{\left(e^{-s_1 N_b h_1} - e^{-s_1 N_b h_2}\right)}, \quad A_2 = \frac{1}{k} + \frac{M}{1+m_1^2},$$

$$s_1 = \frac{N_t(1-m_0)}{N_b(h_1-h_2)}$$

$$c_2 = c_7 + \frac{e^{-s_1 N_b h_1}}{A_2} \left(-G_r A_1 + \frac{B_r N_t A_1}{N_b}\right), \quad c_3 = \frac{B_r s_1}{A_2}$$

$$c_4 = -c_8 \left(-1 - \left(\frac{e^{-s_1 h_1 N_b}}{A_2} + \frac{e^{-s_1 h_1 N_b}}{-A_2 + s_1^2 N_b^2}\right) \left(-A_1 G_r + \frac{A_1 B_r N_t}{N_b}\right) - \frac{G_r - p}{A_2}\right) -$$

$$c_9 \left(-1 - \left(\frac{e^{-s_1 h_1 N_b}}{A_2} + \frac{e^{-s_1 h_2 N_b}}{-A_2 + s_1^2 N_b^2}\right) \left(-A_1 G_r + \frac{A_1 B_r N_t}{N_b}\right) - \frac{G_r - B_r s_1 h_1 + B_r s_1 h_2 - p}{A_2}\right),$$

$$c_5 = e^{-\sqrt{A_2} h_1} \left(-1 - \left(\frac{e^{-s_1 h_1 N_b}}{A_2} + \frac{e^{-s_1 h_1 N_b}}{-A_2 + s_1^2 N_b^2}\right) \left(-A_1 G_r + \frac{A_1 B_r N_t}{N_b}\right) - \frac{G_r - p}{A_2}\right) +$$

$$c_7 \left(e^{\sqrt{A_2} h_2} \left(-1 - \left(\frac{e^{-s_1 h_1 N_b}}{A_2} + \frac{e^{-s_1 h_1 N_b}}{-A_2 + s_1^2 N_b^2}\right) \left(-A_1 G_r + \frac{A_1 B_r N_t}{N_b}\right) - \frac{G_r - p}{A_2}\right) -$$

$$e^{\sqrt{A_2} h_1} \left(-1 - \left(\frac{e^{-s_1 h_1 N_b}}{A_2} + \frac{e^{-s_1 h_2 N_b}}{-A_2 + s_1^2 N_b^2}\right) \left(-A_1 G_r + \frac{A_1 B_r N_t}{N_b}\right) - \frac{G_r - B_r s_1 h_1 + B_r s_1 h_2 - p}{A_2}\right)\right),$$

$$c_6 = \frac{1}{N_b^2 s_1^2 - A_2} \left(-G_r A_1 + \frac{B_r N_t A_1}{N_b}\right),$$

$$c_7 = \frac{-p + G_r - B_r s_1 h_1}{A_2},$$

$$c_8 = e^{(h_2+2h_1)\sqrt{A_2}} c_7, \quad c_9 = e^{3h_1\sqrt{A_2}} c_7$$